Case study: North Sea heavy oil reservoir characterization from integrated analysis of towed-streamer EM and dual-sensor seismic data

Zhijun Du[1] and Kerry Key[2]

https://doi.org/10.1190/tle37080608.1.

Abstract

Integrated analysis of geophysical data can provide valuable information on reservoir properties upon which exploration, appraisal, and development decisions can be made. Here we derive a geophysical reservoir characterization workflow from quantitative interpretation of towed-streamer electromagnetic (EM) and dual-sensor seismic data. The workflow facilitates the reliable extraction of complementary information from two high-fidelity data sets. We demonstrate how the new workflow enables a robust and reliable integration of towed-streamer EM and seismic data with examples from data acquired in a complex geologic region of the North Sea where the heavy oil fields known as Bressay, Bentley, and Kraken (BBK) are located. The BBK discoveries pose several challenges to EM surveying. Airwave coupling in the relatively shallow ocean significantly complicates the reservoir signals. Further, the reservoirs are in close proximity to other high-resistivity features, such as shallow gas in the overburden, the regional Balder Tuff, and granite intrusions. Seismic imaging over these fields is also challenging due to the presence of injectites with steep and irregular geometries. Furthermore, the heavy oil charge means there is no direct hydrocarbon indication in the seismic data due to the low acoustic impedance contrast between the reservoir and surrounding shale.

Introduction

With the depletion of reservoirs in existing fields located both onshore and offshore, the pursuit of hydrocarbons has driven oil and gas exploration and production toward more difficult targets in geographically and geologically complex environments. To be able to assess the hydrocarbon-bearing potential of a formation, exploration is facing increasingly more difficult challenges. Among these challenges is how to accurately image thin reservoirs embedded in a complex geologic background while also accurately mapping the hydrocarbon columns. Historically, exploration wells have been drilled on the basis of seismic data and geologic structure. However, exploration and production technology has evolved immensely over the course of the past several decades; new technological advances now allow exploration to utilize an integrated analysis of multimethod geophysical data sets. Among the various methods available, the integrated analysis of marine controlled-source electromagnetic (CSEM) and seismic data constitutes one of the most robust methodologies for exploration derisking, in particular for geologically challenging areas.

When assessing prospectivity in geologically complex regions, the analysis and interpretation of seismic data provides high-resolution structural images of the subsurface. Marine CSEM data estimate the resistivity of the subsurface and are more sensitive to the presence of hydrocarbons. The integration of seismic with CSEM data can provide subsurface information that is more reliable than when only a single data type is used. However, since seismic and CSEM data sample the earth at very different spatial scales with different sensitivities, the successful integration of the two data types needs to address a number of technical challenges. In this paper, we present a staged quantitative interpretation workflow to make the inversion-based electromagnetic (EM) and seismic integration process more data and information driven and less a priori model driven. The design of the workflow allows for fully leveraging the advantages of the two data sets. The seismic-guided EM inversion method, described in Du and Hosseinzadeh (2014), facilitates an optimal procedure to combine the complementary information from seismic and EM data, with the seismic data best at constraining structure and the EM data best at constraining resistivity.

We present three case studies of integrating dual-sensor seismic data with CSEM data collected using a towed-streamer EM system at the Bressay, Bentley, and Kraken (BBK) fields in the North Sea. By adopting the integrated workflow, we are able to successfully delineate the heavy oil reservoirs of BBK, which are embedded in a complicated geologic environment.

The BBK region and towed-streamer EM data

The BBK heavy oil reservoirs are located on the western edge of the Viking Graben in UK Quadrant 9 of the North Sea (Figure 1). The reservoirs lie within a depth range of approximately 1100–1300 m beneath a shallow water column of approximately 90–130 m. These fields are found in the Dornoch Formation of late Paleocene age. The formation within the block consists of coarse clastics, transitioning to the formation of a prograding delta compound across the eastern boundary of the Shetland Platform. The main source rock is the Kimmeridge Clay Formation (Upper Jurassic), which is encountered within the Viking Graben to the east of the blocks. The targets are the Heimdal sands within the Lista Formation, which consist of a complex, disrupted channel system of unconsolidated and uncemented sands and remobilized injectites. Velocity information from seismic processing shows that the channels/injectites are filled with high-velocity material. This has been confirmed by the appraisal wells that found the in-situ heavy oil (11–12 API) with a viscosity of 1000 cp. The Heimdal heavy oil sands are difficult to image with seismic data alone due to the low acoustic impedance contrast with the surrounding shale.

[1]PGS, Weybridge, Surrey, UK; presently Ocean University of China, College of Marine Geosciences, Qingdao, China. E-mail: zjd202@gmail.com.
[2]Lamont-Doherty Earth Observatory, Columbia University, Palisades, New York, USA. E-mail: kkey@ldeo.columbia.edu.

In 2012, PGS conducted a towed-streamer EM survey over the BBK heavy oil fields (Figure 1). The towed-streamer EM acquisition system consisted of an approximately 7.7 km receiver cable deployed at 50–100 m water depth and a 1500 A, 800 m long bipole source towed at 10 m depth. With a 4-knot towing speed, the acquisition pattern was based on a source signal every 250 m and 44 unique receiver positions for each "shot." Compared to a conventional node-based marine CSEM system in which the receivers are very sparsely placed on the seafloor in a line or areal pattern approximately 1 km apart, the highly sensitive receiver electrodes housed in the streamer were able to densely sample the subsurface with an average offset interval of approximately 160 m over offset ranges of approximately 700–7595 m. Additionally, whereas conventional seafloor EM receivers use 10 m long electric field sensors, the towed system uses variable receiver length sensors spanning a range of 200–1100 m, resulting in high-sensitivity measurements. The towed-streamer EM system provides the dense sampling, data quality, and signal-to-noise ratio that are required for imaging challenging targets in a shallow-water environment.

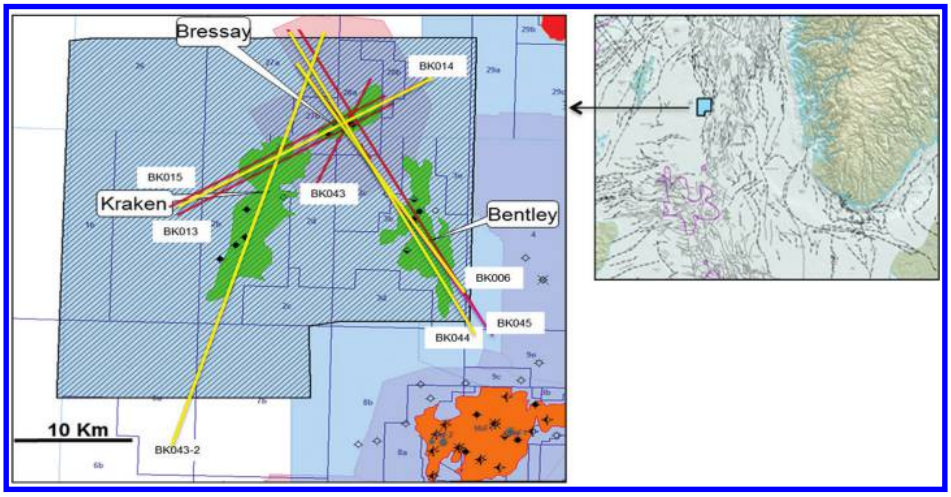

Figure 1. Map showing the towed-streamer EM survey lines collected in 2012 over the BBK reservoirs in the North Sea. Four of the survey profiles (yellow lines) are used in this study.

Towed-streamer EM data processing methodology

The BBK EM data were inverted using the MARE2DEM code (Key and Ovall, 2011; Key, 2016), which was recently modified and improved to accurately and efficiently handle towed-streamer EM data. MARE2DEM uses a regularized nonlinear inversion built around a 2.5D parallel adaptive finite element algorithm (Key and Ovall, 2011; Key et al., 2014; Key, 2016). The finite element approach uses automatic mesh generation and goal-oriented adaptive refinement to generate a mesh that gives accurate EM responses for a given suite of data and model parameters. Nonlinear inversion is carried out using a parallel implementation of the Occam method (Constable et al., 1987), a regularized variant of Gauss-Newton minimization that automatically determines the optimal trade-off between data fit and regularization during each inversion iteration.

Computation considerations

Modification and improvement of MARE2DEM was necessary to ensure the accurate modeling and inversion of towed-streamer EM data and to utilize the data density. These developments resulted from three main features of the acquisition system:

1) The towed-streamer EM system uses an 800 m long transmitter and offset-dependent 200–1098 m long receiver dipoles. The EM fields depart significantly from those of point dipoles due to "bipole" effects. Accurate modeling of the finite length and orientation of both the source and receivers is necessary.
2) Towed-streamer EM data have dense inline sampling of the horizontal electric field. For a typical acquisition, the spatial data density is around four times denser than a conventional seafloor node CSEM acquisition (Key et al., 2014). While the increased data density improves the stability of the inversion, and importantly the quality of the subsurface resistivity model, the computational burden of inversion is also significantly increased.
3) The commonly used EM reciprocity theorem, in which the modeled transmitter and receiver dipoles are interchanged to reduce the number of linear systems required to solve the forward problem and lessen the computational load, is not applicable for the towed-streamer system since the towed-receiver array is moving together with the transmitter.

The modeling and inversion of towed-streamer EM data is computationally intensive and challenging. Typically, it is about 10 times more computationally intensive than modeling conventional seafloor node CSEM data. To alleviate the computation burden so the problem can fit into the available computation facilities, we decimated the BBK data set by desampling the source positions by a factor of two and the receiver positions for each source by three. The reprocessed data set consists of source-receiver offsets of 743–7457 m and six frequencies from 0.2 to 1.2 Hz with an increment of 0.2 Hz, giving about 10,000 data for each towline inversion.

Unconstrained EM inversion

We began with unconstrained blind inversions (those that do not incorporate field geology constraints) for both isotropic and anisotropic resistivity, with all inversions starting from a uniform half-space model. Convergence is often accelerated if the uniform resistivity of the start model is chosen so that the amplitude levels of the measured and modeled data are similar at the start of the inversion. The only fixed model parameters are sea resistivity and seafloor topography. Sea resistivity was estimated from temperature profiles measured with expendable bathythermographs deployed daily by the survey support vessel at different locations throughout the survey area. Seafloor topography was measured by the survey vessel's echo sounder.

We parameterized the model domain with a dense grid of 10,000–20,000 unknown resistivity parameters (depending on the profile length) from the seafloor to 2.5 km depth. We applied a 1% error floor to the data and found that most of the survey profiles could fit a root mean squared (rms) misfit of about 0.8 to 1.0 within about 10–15 Occam iterations, requiring a few hours of run time on 320 processors.

Isotropic inversion. In a shallow-water setting (e.g., less than about 500 m), a number of recent studies have shown that the inline component of the electric field induced by a horizontal electric dipole is sensitive to anisotropy and can successfully recover both the horizontal and vertical resistivities (e.g., MacGregor and Tomlinson, 2014). In this regard, we examine the performance of recovering subsurface anisotropy from using towed-streamer EM data. Our test consisted of isotropic inversion of synthetic data of a model containing uniform sediments with 1.0 ohm-m horizontal and 1.5 ohm-m vertical resistivity, based on the anisotropy experienced along line BBK006 (Bhuiyan et al., 2013). An initial blind inversion for isotropic resistivity resulted in strong horizontal bands of alternating resistive and conductive layers, with some evidence for increased resistivity at the locations of the reservoirs near 1 km depth. In Figure 2a, we show results of the isotropic inversion of line BK006 real data. Since the resulting inversion showed similar stripes to that in synthetic inversion, we conclude that the stripes are an artifact that creates an effective bulk anisotropy by means of stacked isotropic layers of alternating resistivity (e.g., Newman et al., 2010). We concluded that the towed-streamer EM data have high sensitivity to anisotropic resistivity. Hence, in our further analysis we only apply anisotropic inversion.

Anisotropic inversion. Figures 2b and 2c show anisotropic inversion's horizontal and vertical resistivity results. Anisotropic inversion clearly resolves the presence of the Bentley and Bressay reservoirs. Figure 2d shows the vertical to horizontal anisotropy ratio for this inversion, which reveals a ubiquitous layer at about 0.5 km deep that displays a factor of two anisotropy ratio, whereas the rest of the model, except the reservoirs, is nearly isotropic (ratio equal to one). The significant shallow anisotropy is most likely caused by interbedding of shale with brine sand in the overburden, as suggested by nearby well-log analysis.

Figures 3a, 3b, and 3c show the anisotropic inversion results (for brevity only the vertical resistivity) from the three selected survey lines (BK006, BK014, and BK043-2), which cross over BBK, respectively (yellow lines in Figure 1).

Unconstrained inversion seeks the smoothest model that fits the data, where smoothness is measured in a first derivative sense (Constable et al., 1987). Although the unconstrained inversions do not resolve complex or highly detailed small-scale features, they allow the assessment of the class of structures to which the data are most sensitive and the variations in these structures across the area. The inversions have faithfully recovered the resistive basement, which is not unexpected given that it has the largest impact on data responses. They have also revealed several localized large bodies with significantly increased resistivity in the overburden. While these increases are located at the lateral positions of the known BBK reservoirs, their depths are inconsistent with the reservoirs.

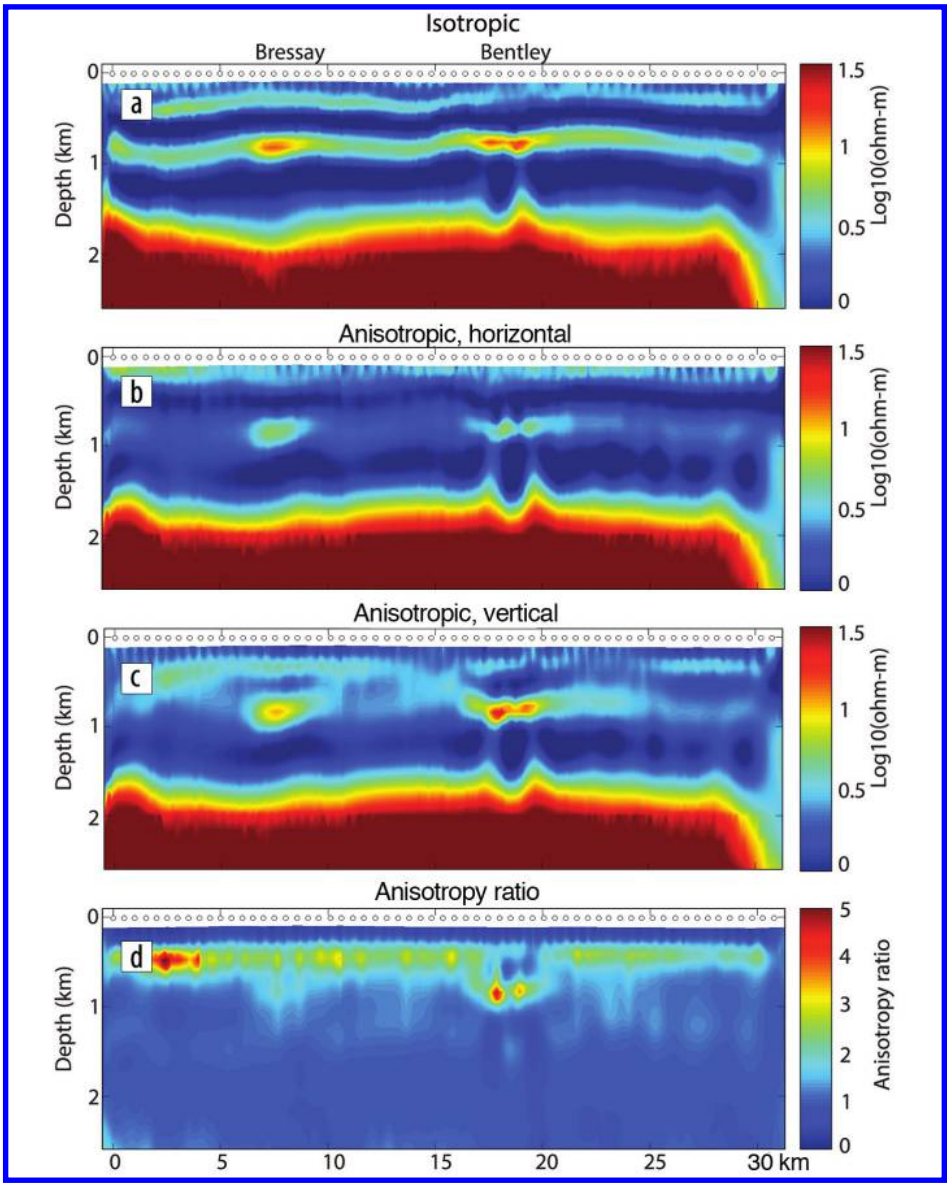

Figure 2. The unconstrained inversions for towline BK006. (a) Isotropic inversion shows significant horizontal bands of high resistivity that mask the presence of the two reservoirs. Anisotropic inversion, for the (b) horizontal and (c) vertical resistivity, clearly images the discrete reservoir resistors. (d) The vertical/horizontal anisotropy ratio shows that anisotropy reaches a factor of two in a ubiquitous layer approximately 0.5 km deep.

Seismic-guided EM inversion

The use of unconstrained inversion recovered a useful, informative, smoothed image of subsurface resistivity but did not resolve complex structures. It is well known that for thin resistive layers, the quantity best constrained by CSEM data is transverse resistance (resistivity-thickness product); thin resistive layers are often smeared vertically by inversions so they are less resistive and much thicker than the actual structure. To integrate towed-streamer EM and dual-sensor seismic data, we introduce a seismic-guided EM inversion (Du and Hosseinzadeh, 2014; McKay et al., 2015). The higher resolution of the seismic image makes it possible to suggest the most appropriate locations of potential resistivity contrasts and thereby helps resolve the resistivity-thickness ambiguity, resulting in improved estimates of bulk resistivity. The integration of seismic data with EM data can overcome the limitations of each method, and the strengths of each can be fully exploited.

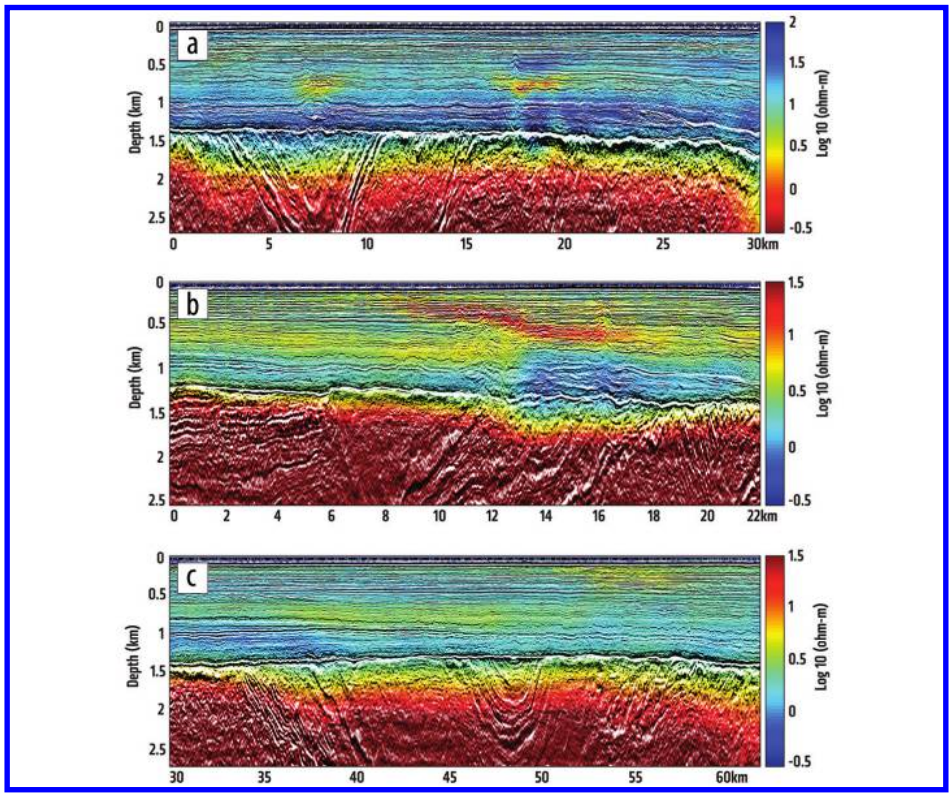

Figure 3. Resulting vertical resistivity from the 2.5D unconstrained anisotropic inversions of lines (a) BK006 (over Bressay and Bentley), (b) BK014 (over Bressay), and (c) BK043-2 (over Kraken) corendered by the coincident depth-converted full-stack broadband dual-sensor seismic data.

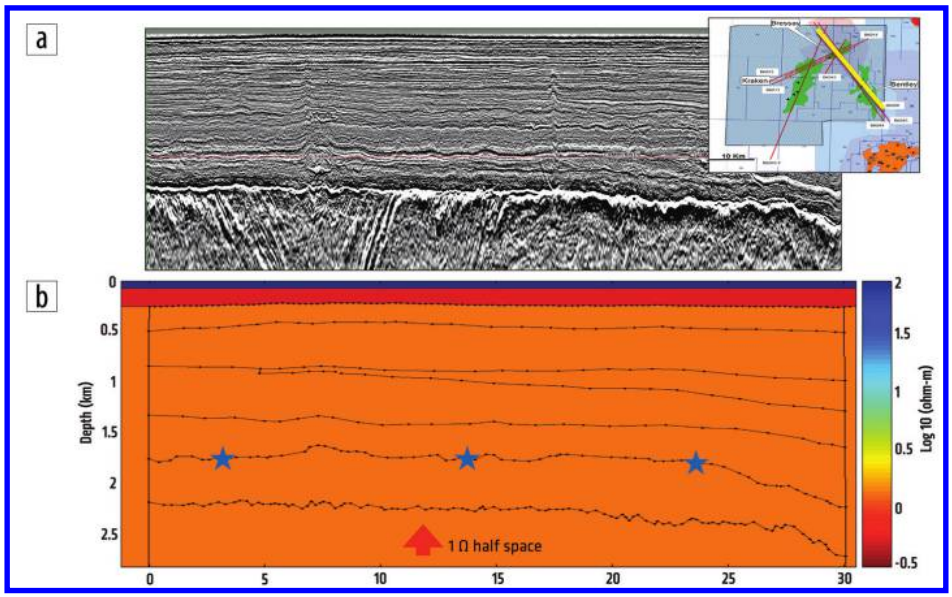

Figure 4. An illustrative setup for conducting seismic-guided inversion for line BK006 (yellow line in the inset). (a) The coincident broadband dual-sensor seismic section in depth. (b) The interpreted seismic horizons extracted from the top and adopted for guiding the EM inversion. The stars indicate the seismically defined top reservoir interface.

We set up the seismic-guided inversion of line BK006 to have an isotropic 1 ohm-m half-space background, as shown in Figure 4. While the boundaries between the interbedded sands and shales in the overburden were delineated by poststack dual-sensor seismic data, for the anisotropic resistivity variations in the layers above the top reservoir (indicated by the star), we placed minimum and maximum bounds on the resistivity-free parameters using a nonlinear transform of the model parameter space (e.g., Key, 2016). The bounds were set using the lowest (0.3 ohm-m) and highest (3 ohm-m) resistivity, as constrained by the previous unconstrained anisotropic 2.5D inversions (Figure 3a), while the remaining regions had no bounds on the resistivity-free parameters. Note that the seismic boundaries have been adopted only for the purpose of "guiding" EM inversion since the geologic interfaces mapped by seismic may or may not be potential EM resistivity boundaries. The resistivity-free parameters on each side of the boundaries can vary freely within their prescribed minimum and maximum bounds, as required to fit the data. Consider uncertainties in the seismic data from the time-to-depth conversion, and also that a reservoir can be hydrocarbon-charged to an unknown degree, corresponding to the spill point or less. The seismic-guided approach gives inversion the flexibility to place a resistivity contrast away from a seismic interface boundary if needed to satisfy the EM data fit. In this way, we allow the inversion to use both the seismic horizons and the parameter constraints determined from the unconstrained inversion as guides only, while still providing sufficient model regularization for stable inversion.

Case study 1: Bressay and Bentley. The resulting resistivity model of the seismic-guided inversions for line

BK006 is shown in Figure 5a. The results show significantly improved depth location and vertical resolution of the targets compared to the unconstrained inversion (Figure 3a), demonstrating the power of data integration. By using seismic to guide the EM inversion, the results of the inversion now better match the reservoir depths and lateral geometries of Bressay and Bentley. The prominent resistivity anomalies coincide with the positions of the main target structures that we identified by detailed analysis of the seismic data.

Case study 2: Bressay. Figure 5b shows the vertical resistivity of the final result of the seismic-guided inversion for line BK014, which crosses the lateral extent of Bressay Field. Compared to the unconstrained inversion (Figure 3b) where the thin Bressay reservoir was not resolved, the seismic-guided inversion has retrieved a prominent high-resistivity anomaly at the depth and lateral position of the known Bressay reservoir. Furthermore, by comparing it to the result obtained by the unconstrained inversion (Figure 3b), both inversions have revealed a large shallow resistive body in the overburden, in the depth range of approximately 500–800 m between the profile distance of approximately 8 and 18 km. The body is most likely due to shallow gas: there is obvious seismic amplitude brightening and there is a clearly visible chimney-like vertical gas-leakage path from the top reservoir to the body that crosscuts primary seismic reflections. Therefore, a shallow gas body may be formed by gas leakage from the top of the reservoir (Figures 3b and 5b).

Case study 3: Kraken. The Kraken reservoir overlies the resistive basement, with a vertical separation of less than approximately 200 m. In this case, the unconstrained inversion was unable to isolate the target, which is instead merged into the deeper basement structures (Figure 3c). For conducting seismic-guided inversion for line BK043-2, we have adopted a seismic horizon that defines the top of the Heimdal sand as a "cut" to break the inversion's model roughness penalty at the top of the reservoir (a sharp contrast in resistivity is allowed here). Figure 5c shows the final inverted resistivity model, indicating that the cut (the thin white line) is helpful to constrain the reservoir, but has no adverse effect on other parts of the horizon where the cut was also applied (along the surface seismically defined as the top of the reservoir sand). The cut also has little effect on the inversion's retrieval of the background structure, as evidenced by comparing unconstrained (Figure 3c) to seismic-guided inversion (Figure 5c).

The line BK043-2 seismic-guided inversion result displays a localized resistivity anomaly coinciding with the location of the known Kraken reservoir (Figure 5c). The seismic-guided inversion was able to vertically separate the reservoir from the basement with further help of the cut, while the basement boundary exhibits lateral resistivity variations that closely follow the seismic amplitudes.

Case study 4: Kraken and Bressay. By focusing on the seismically constrained subsurface structures of interest, we investigate the consistency of the lateral variation in resistivity in the overburden (depths between approximately 300 and 1000 m) over Kraken and Bressay, as shown by the results from the inversion of lines BK043-2 and BK014, respectively (Figures 5c and 5b). We simply stitched the two sections together at the location where they cross each other to form an arbitrary line. The resistivity profile for this newly formed arbitrary line, achieved simply by laying the two individual inversion results side by side, is shown in Figure 6b. What we observe is a consistent seamless link of the lateral structure from two independent models. The concatenated model displays an overall picture of the regional geology; in particular, it highlights the resistivity variations in the shallow section and their correlation with overburden structures (Figure 6).

Data density and target recoverability

Similar to line BK006, line BK045 seismic-guided inversion recovered resistive targets at the depth and lateral locations of the known reservoirs of Bressay and Bentley. In Figure 7a, we show the vertical resistivity section in the vicinity of the Bentley reservoir. (For brevity we only show a portion of the full survey line.) Here the inversion has introduced a few "holes" of low resistivity extending deeply into the basement, for which there are no plausible geologic explanations. In addition, in the southern part of Bentley (right side of the inversion image), in a vertical sense, the resistive

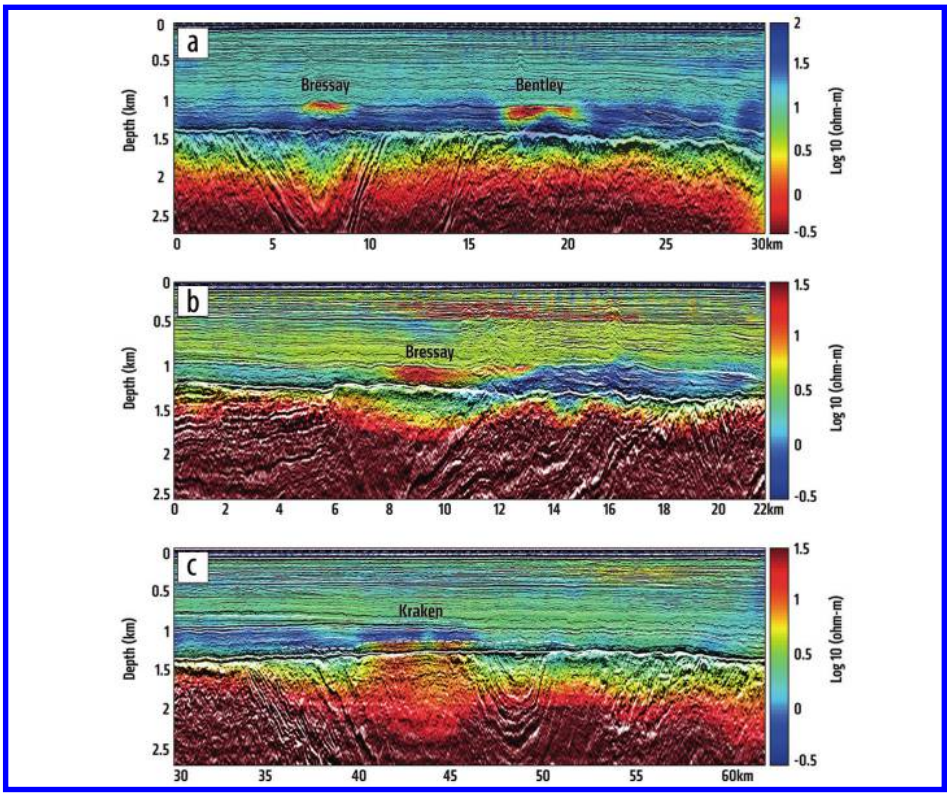

Figure 5. Resulting vertical resistivity from the 2.5D seismic-guided inversions of lines (a) BK006 (over Bressay and Bentley), (b) BK014 (over Bressay), and (c) BK043-2 (over Kraken), corendered by the coincident depth-converted full-stack broadband dual-sensor seismic data.

features have not been recovered but are partially smeared into the basement. We suspect this was probably due to incomplete data coverage (a cost from the heavy desampling of the data set). For the case of a 2D structure, MacGregor and Tomlinson (2014) and Tshering et al. (2015) conducted independent studies for the issue of "recoverability" related to data density by using synthetic data sets from node and towed-receiver acquisitions, respectively. One of the important features revealed by these studies, regardless of the acquisition system, is that target recoverability depends heavily on spatial sampling, or data density, and more fine-scale resistive structures could only be recovered from a dense data set.

To further investigate the result of BK045 inversion, we chose to invert only part of the line and to use the full data density rather than subsampling the sources by two and the receivers by three, as we did in our previous inversion. This allows us to study how towed-streamer spatial dense sampling can possibly improve resolution and precision in comparison to those derived from coarser data (Figure 7a). We reparameterized the model domain for the portion of the line covering Bentley with a denser triangular grid of approximately 23,200 cells with 46,400 (anisotropic) unknown resistivity parameters from the seafloor to a depth of 2.5 km. This setup is about half the lateral extent of the inversion grid used in the previous inversion (Figure 7a). The inversion domain is now only about 20 km long (covering the line segment between approximately 25 and 45 km), which allows us to invert data for every source-receiver offset and to process the entire recorded data set for a refined model grid.

Figure 7b shows the final vertical resistivity model, which fits to an rms misfit of about 1.03. Comparison of the previous inversion (Figure 7a) with the new inversion (Figure 7b) shows that more fine-scale resistive structures have now been resolved. Overall, the new inversion is clearly a significant improvement from the previous inversion. The inversion with more data and a finer model parameterization improves the separation of the reservoir from the basement while retrieving the basement boundary with lateral resistivity variations that more closely follow the amplitude of seismic reflections. In addition, some additional improvements at the reservoir level are now present. Bentley is now imaged as a vertically compact resistivity anomaly, centrally connected by two high anomalies, side by side, forming a "w" shape. Later we investigate and further discuss the Bentley resistivity anomaly.

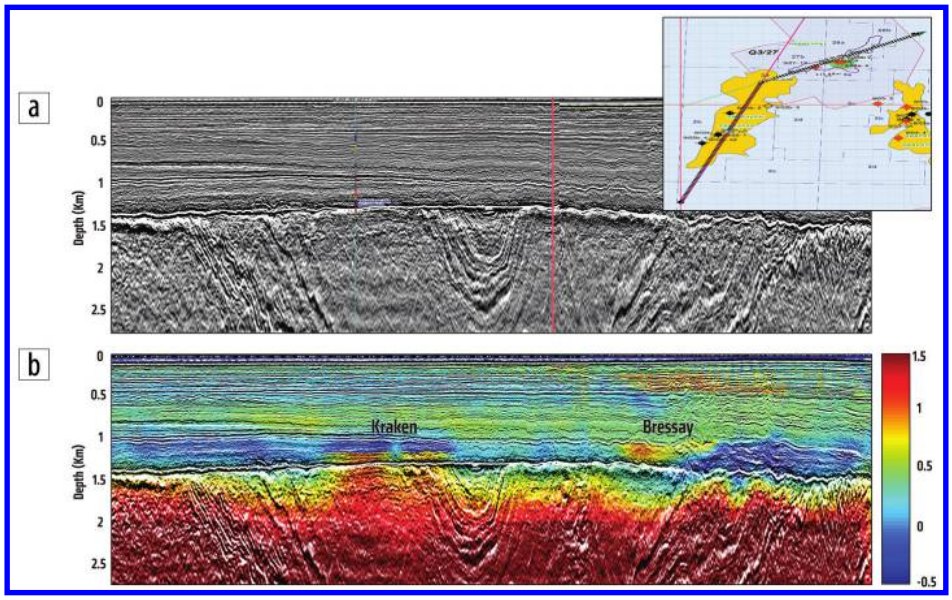

Figure 6. The arbitrary line, as indicated in the inset, obtained by stitching the survey lines BK043-2 and BK014 together at the location where they are crossing each other. (a) The coincident broadband dual-sensor seismic section in depth. (b) The vertical resistivities formed by merging sections of the lines BK043-2 and BK014 seismic-guided inversions together (Figures 5c and 5b).

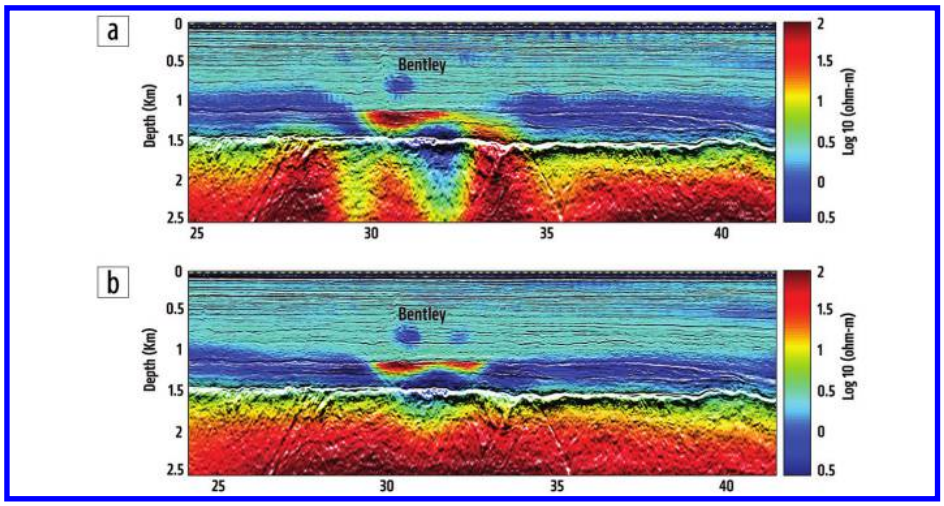

Figure 7. Resulting vertical resistivity from the seismic-guided inversion of line BK045 corendered by the coincident depth-converted full-stack broadband dual-sensor seismic data. (a) Inversion of the desampled data. (b) Inversion of the fully sampled data set.

Integrated analysis

Hydrocarbons are typically found in traps, where stratigraphy or geologic structure keeps oil and gas from migrating vertically or laterally. Regarding this, knowledge of reservoir geometry is important in quantifying recoverable hydrocarbon resources. The reservoir thickness and areal extent are relevant parameters that serve as inputs for reservoir characterization volumetric analysis (i.e., estimation of the total hydrocarbons in place).

We continue our investigation for line BK045 from the preceding section. Integrated analysis combines the result of seismic reservoir characterization and uses the mapped reservoir sands from seismic interpretation. Figure 8a shows the reservoir top horizon in plan view and superimposed is the outline of the Bentley lateral extent (denoted by a

polygon), both resulting from seismic reservoir interpretation. Line BK045 crosses the long axis of Bentley. Figure 8b shows a 3D view displaying the inverted BK045 resistivity in the vertical plane and the seismic interpreted outline of the Bentley reservoir in plan view. It is evident that high-magnitude resistivity (in red) is restricted to within the boundary of the seismic-delineated reservoir. In addition, it explains the "w"-shaped Bentley 2D resistivity distribution, where the center of the image is concave (marked by a red arrow) due to the survey line BK045 passing closely through the boundary (the edge of the reservoir) where the sand is less resistive. The integration of seismic with CSEM data provides us with a complementary image primarily related to the lithology and fluid content within the reservoir.

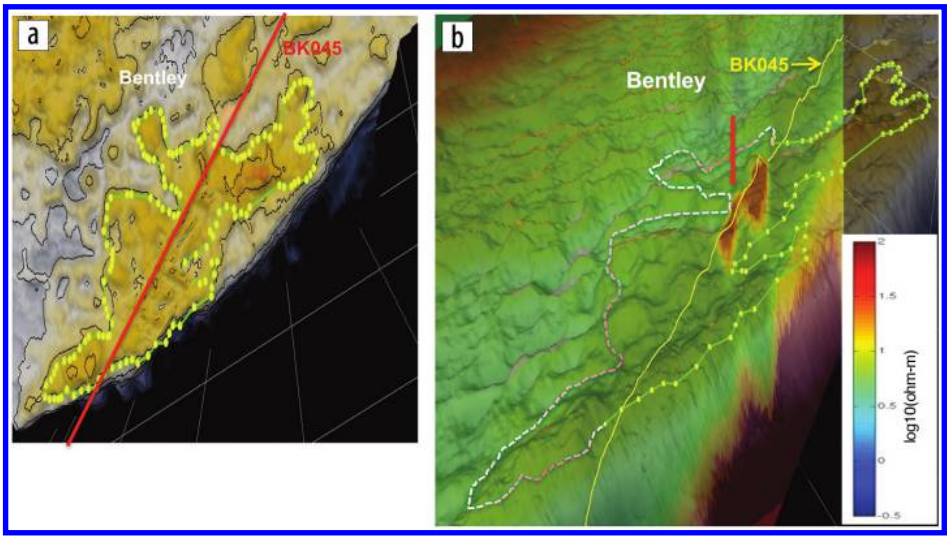

Figure 8. (a) The plan view shows that line BK045 (red line) crosses the long axis of Bentley, together with the reservoir top horizon and seismically delineated reservoir sand bodies (yellow polygons). (b) The vertical plane displays inverted BK045 vertical resistivity, as shown in Figure 7b (the thin yellow line is the BK045 trajectory as indicated by the red line in [a]). The plan view shows the reservoir top horizon (green). The polygon (replotted from [a]) indicates that the outlet of Bentley reservoir resulted from seismic reservoir interpretation.

Well logs provide a higher resolution measurement of the properties of a reservoir and the overburden strata at the location of the well. A number of exploration wells are available, mostly located in the northern part of Bentley. The oil water contact (OWC) determined by these wells is fairly stable and located at depths of approximately 1136–1138 m. We could, therefore, reasonably conclude that the OWC is flat in the northern part of Bentley. In Figure 9, we expand this assumption to the southern part, positing that the sand bodies below the OWC (indicated by a gray plane) are most likely water-saturated sand containing only residual oil. This is consistent with the high resistivities (denoted by pink dots in Figure 9b)

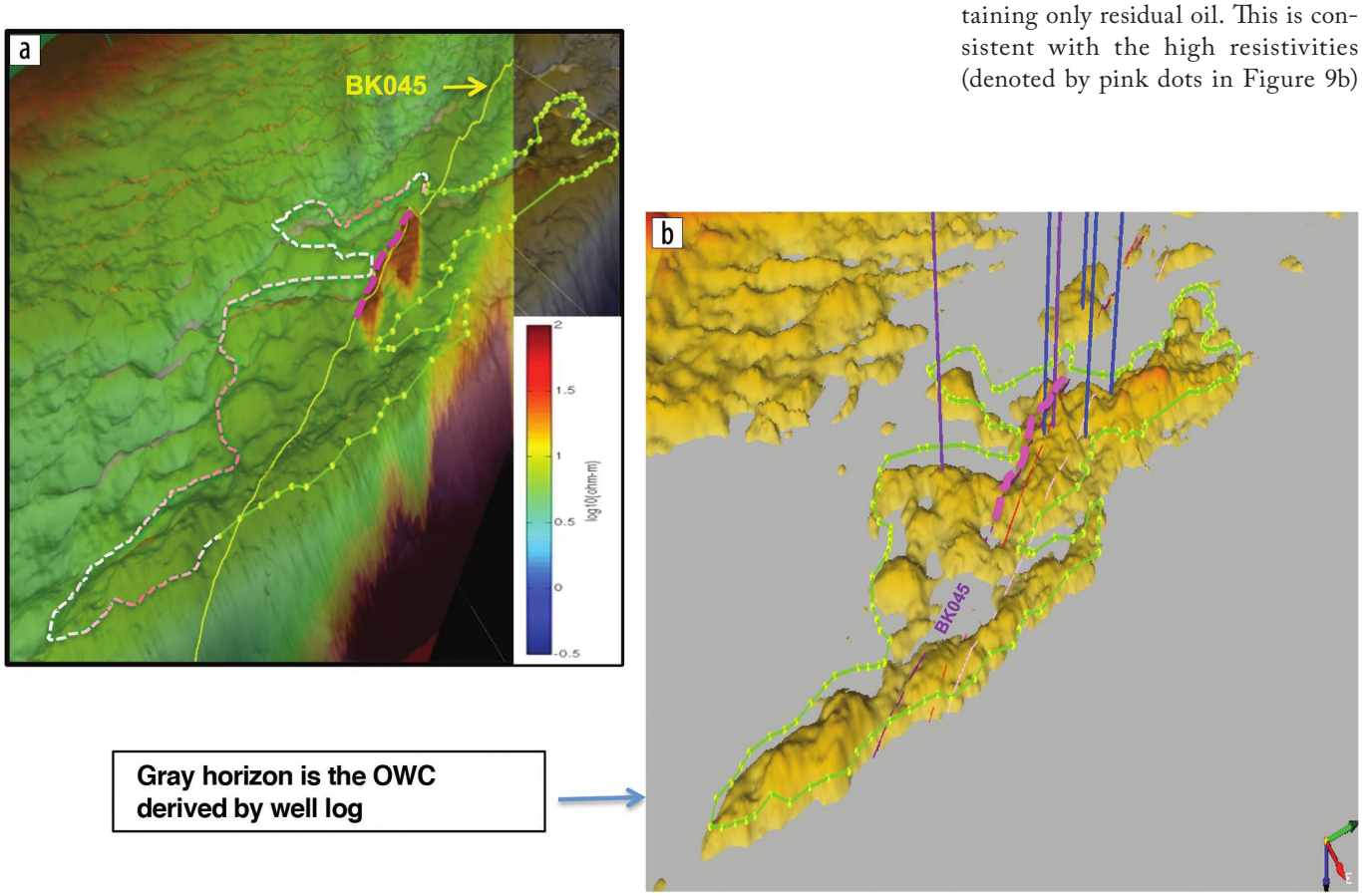

Figure 9. (a) Continued from Figure 8, where the pink dots delineate the highest resistivities along the line. (b) Reservoir top horizon overlain by the OWC (gray). A thin purple line indicates the footprint of line BK045, whereas the pink dots denote the positions of highest resistivity. Vertical lines indicate well paths for the available exploration wells.

being only overlain with sand bodies above the OWC, supporting the presence of dense oil in place.

In Figure 9, we observe good agreement between seismic reservoir interpretation, well logs, and EM inversion. The resistivity anomalies delineate the hydrocarbon charged from brine-saturated sands within the reservoir sand body, determined by seismic reservoir interpretation. In our staged integration workflow, seismic, well log, and towed-streamer EM technologies each make unique contributions that when combined give more comprehensive results than possible with any of these data sets when analyzed independently. An integrated workflow such as this provides a powerful tool for reservoir characterization in order to discriminate between lithology and fluid properties. Moreover, it can serve as veritable inputs for reservoir volumetric analysis, i.e., estimating the total volume of hydrocarbon in place.

Conclusions

We present an improved reservoir characterization workflow based on integrating multimethod geophysical data sets of towed-streamer EM, well logs, and dual-sensor seismic data. We applied the workflow to process and interpret a towed-streamer EM survey data set acquired over BBK, a complex geologic area in the North Sea, in order to illuminate three heavy oil reservoirs.

By using a staged integration workflow where seismic, well log, and towed-streamer EM technologies make selective contributions with their individual strengths, we demonstrated that the integrated analysis results in reservoir characterization that can discriminate between lithology and fluid properties, and can discern hydrocarbon from brine sands. Because the integration is purely data driven with no assumptions about the existence, size, and shape of reservoirs in the workflow, the workflow can be adopted in exploration frontier settings where CSEM and 3D seismic data coexist for prospect ranking and derisking. TLE

Acknowledgments

We would like to thank Vinnie Papenfus for drafting the figures and PGS for permission to publish this work.

Corresponding author: zjd202@gmail.com

References

Bhuiyan, A., R. Sakariassen, Ã. Hallanger, and A. McKay, 2013, Modeling and interpretation of CSEM data from Bressay, Bentley, and Kraken area of East Shetland Platform, North Sea: 83rd Conference and Exhibition, SEG, Expanded Abstracts, 815–819, https://doi.org/10.1190/segam2013-1409.1.

Constable, S. C., R. L. Parker, and C. G. Constable, 1987, Occam's inversion — A practical algorithm for generating smooth models from electromagnetic sounding data: Geophysics, **52**, no. 3, 289–300, https://doi.org/10.1190/1.1442303.

Du, Z., and S. Hosseinzadeh, 2014, Seismic guided EM inversion in complex geology — Application to the Bressay and Bentley heavy oil discoveries, North Sea: 76th Annual Conference and Exhibition, EAGE, Extended Abstracts, https://doi.org/10.3997/2214-4609.20141250.

Key, K., 2016, MARE2DEM: A 2-D inversion code for controlled-source electromagnetic and magnetotelluric data: Geophysical Journal International, **207**, no. 1, 571–588, https://doi.org/10.1093/gji/ggw290.

Key, K., and J. Ovall, 2011, A parallel goal-oriented adaptive finite element method for 2.5-D electromagnetic modelling: Geophysical Journal International, **186**, no. 1, 137–154, https://doi.org/10.1111/j.1365-246X.2011.05025.x.

Key, K., Z. Du, J. Mattsson, A. McKay, and J. Midgley, 2014, Anisotropic 2.5D inversion of towed streamer EM data from three North Sea fields using parallel adaptive finite elements: 76th Annual Conference and Exhibition, EAGE, Extended Abstracts, https://doi.org/10.3997/2214-4609.20140730.

MacGregor, L., and J. Tomlinson, 2014, Marine controlled-source electromagnetic methods in the hydrocarbon industry: A tutorial on method and practice: Interpretation, **2**, no. 3, SH13–SH32, https://doi.org/10.1190/INT-2013-0163.1.

McKay, A., J. Mattsson, and Z. Du, 2015, Towed streamer EM — Reliable recovery of sub-surface resistivity: First Break, **33**, no. 4, 75–85.

Newman, G. A., M. Commer, and J. J. Carazzone, 2010, Imaging CSEM data in the presence of electrical anisotropy: Geophysics, **75**, no. 2, F51–F61, https://doi.org/10.1190/1.3295883.

Tshering, T., K. F. Bergh, J. Malmberg, and J. Mattsson, 2015, Improved vertical and lateral resolution in inverted towed streamer EM data as a function of increased data density: Presented at 24th International Geophysical Conference and Exhibition, ASEG-PESA.